The Morphology and 3-D Structures of the Ionized, Molecular, and Dust Components of Plnaetary Nebulae

Sun Kwok

University of Hong Kong `sunkwok@hku.hk`

Summary. The morphology of the ionized, molecular, and dust components of planetary nebulae can be traced by optical, infrared and mm/submm observations. Recent progresses in mm/submm interferometry, mid-infrared imaging with active optics, and optical imaging spectroscopic observations have allowed the separate mapping of all these components. The intrinsic 3-D structures of planetary nebulae are discussed from the result of these observations.

Key words: keyword list

1 Where is the "dark matter"?

While our common perception of planetary nebulae (PNe) is dominated by optical images arising from line emissions from the ionized region, we now realize that the optical images do not represent a complete picture of the nebulae. Millimeter and submillimeter observations have found that many PNe have extensive molecular components with masses many times that of the ionized component. PNe typically contain 10^{-1} $M_\odot$ of ionized gas, but the amount of molecular gas can be as high as several $M_\odot$. Infrared observations have revealed that a large fraction of the energy emitted by PNe is from the dust component (Fig. 1). The observations molecular and dust components, the "dark matter" in PNe, are therefore crucial in our understanding of the structure and composition of PNe.

However, until recently, the distributions of molecular and dust components in PNe were practically unknown. Advances in mm/submm interferometry and high-resolution mid-infrared imaging have made possible the imaging of the molecular and the dust components respectively. Submm arrays such as *PdBI, CARMA, SMA*, and *ALMA* can achieve subarcsec angular resolutions and are capable of mapping the distribution of the emission regions of molecular lines, free-free continuum, and dust continuum. Large infrared telescopes with adaptive optics capability can obtain infrared maps in the 10 and 20 μm
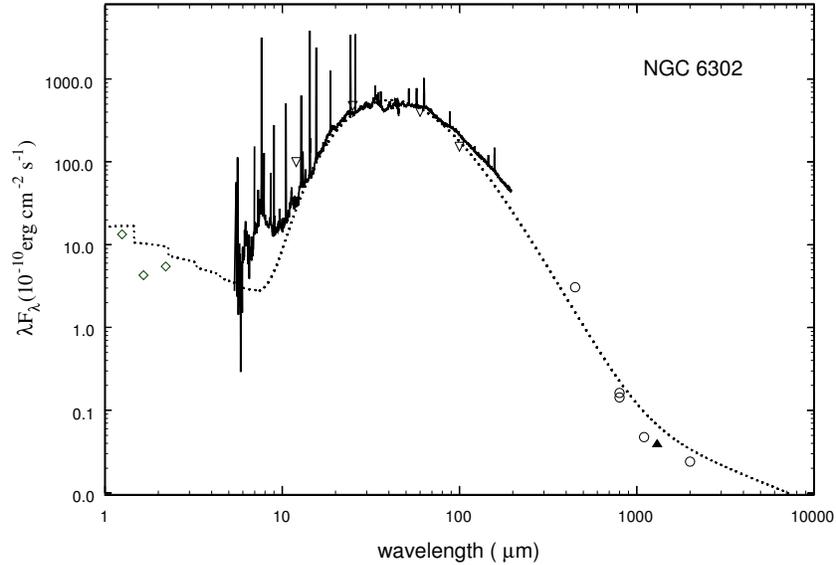
Fig. 1. The spectral energy distribution of NGC 6302. The ionized component manifests itself in fine structure emission lines in the ISO SWS and LWS spectra (shown as solid line), in the bound-free continuum in the near infrared, and in free-free continuum in the radio and mm wavelengths. The strong emission peak between λ 10 μm and 1 mm is due to dust emission. The transition from dust to free-free emission occurs at $\sim$1 mm. The inverted triangles, diamonds, open circles, and the filled triangle are the IRAS Point Source Catalog fluxes, JHK ground-based photometry, JCMT photometry, and SMA measurements, respectively. The dotted line is a model continuum spectrum including contributions from bound-free, free-free, and dust emissions.

atmospheric windows with subarcsec resolution, and with narrow filters able to separate the emission regions arising from ionic fine-structure lines, aromatic infrared bands (AIB), silicate emission, and the dust continuum. These results allow us to compare the relative spatial distributions of the ionized, molecular, and dust emission regions.

2 Submm Imaging

NGC 7027 is the first PN to have its molecular envelope mapped by a millimeter interferometer and comparisons with the optical and radio continuum maps show a clear photodissociation region separating the ionized and molecular gas components [4]. For NGC 6302, submm observations have found an expanding molecular torus, which correspond to the dark lane separating the optical bipolar lobes [14, 2].

Fast molecular outflows can be detected by single-dish mm/submm observations from the extended wings of the CO profile. The first detection of fast molecular outflows in PPNe and PNe was in AFGL 618, where the CO wings extend to ± 200 km s^{-1} [3]. High-resolution CO $J = 6 - 5$ images of AFGL 618 show that the high-velocity components lie along the optical lobes [13]. In NGC 2440, the CO outflow has been imaged to correspond to one pair of the optical bipolar lobes [20] (Fig. 2).
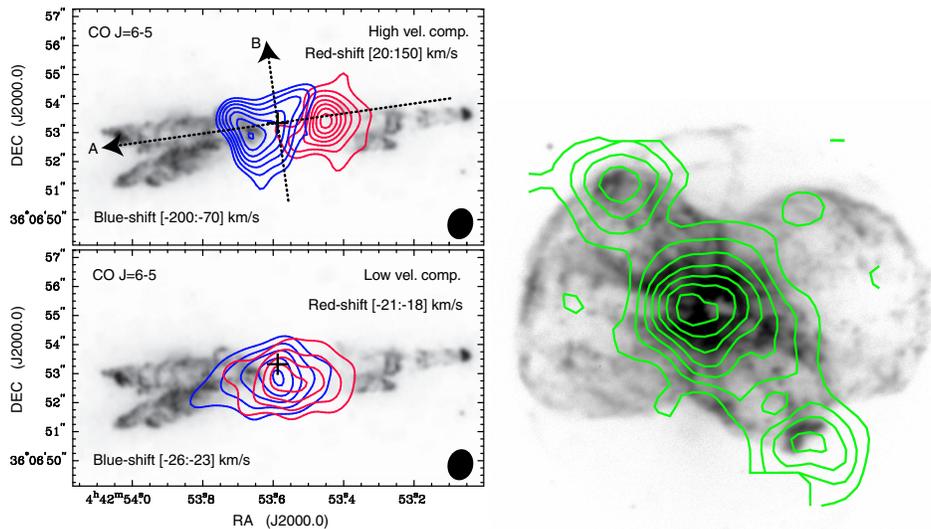
Fig. 2. Left: SMA CO $J = 6 - 5$ (shown in contours) high- (top panel) and low- (bottom panel) velocity components emission superimposed on the HST Hα image of AFGL 618 [13]. Right: CO $J = 3 - 2$ emission (shown in contours) in NGC 2440 observed with the *JCMT* overlaid on a [N II] image taken at the *CFHT*[20].

Due to the interaction between the fast outflow and the remnant AGB molecular envelope, much of the observed CO emission is likely to arise from swept-up mass rather than from the outflow itself. Therefore it is not trivial to derive the mass and velocity of the outflow from the observed CO brightness and line profiles. An over simplistic interpretation will lead to an over estimate of the mass loss rate and an underestimate of the outflow velocity [5].

3 Mid-Infrared Imaging

The Multiband Imaging Photometer (MIPS) of the *Spitzer Space Telescope* offers angular resolutions of 6, 18, and 40 arcsec at 24, 70, and 160 μm respectively, and is capable of resolving the equatorial torus of large bipolar nebulae. Observations of NGC 2346 [19] shows that warm dust (as evidenced by emission at 24 μm) is present in both the bipolar lobes and in the torus, cool dust (as evidenced by emission at 70 μm) is mostly located in the edge-on equatorial torus, and the cold dust (as evidenced by emission at 160 μm) is distributed over a spherical region, probably arising from the remnant of the AGB wind.

For an infrared-optimized ground-based telescope equipped with adaptive optics such as the 8-m *Gemini Telescopes*, near diffraction-limited resolution can be achieved. For the Thermal Region Camera Spectrograph (T-ReCS) and Michelle infrared imagers on the Gemini Telescopes, this corresponds to $\sim 0.''4$. With image deconvolution using an observed point spread function, the angular resolution can be further improved to $< 0.''2$ [12].

For PNe and PPNe, imaging at 10 and 20 μm show dust emissions both in the lobes and in the torus [22]. Since the dust torus is generally defined by a dark lane in the optical image, infrared imaging provides a direct determination of the size and orientation of the torus. An interesting case is IRAS $17441-2411$ where the the orientation of the axis of the infrared torus is found to be offset by $23°$ from the bipolar axis (Fig. 3). If the torus is responsible for or related to the collimation of the bipolar outflow, this raises the possibility that the outflow has undergone precession over the last 100 years [21].
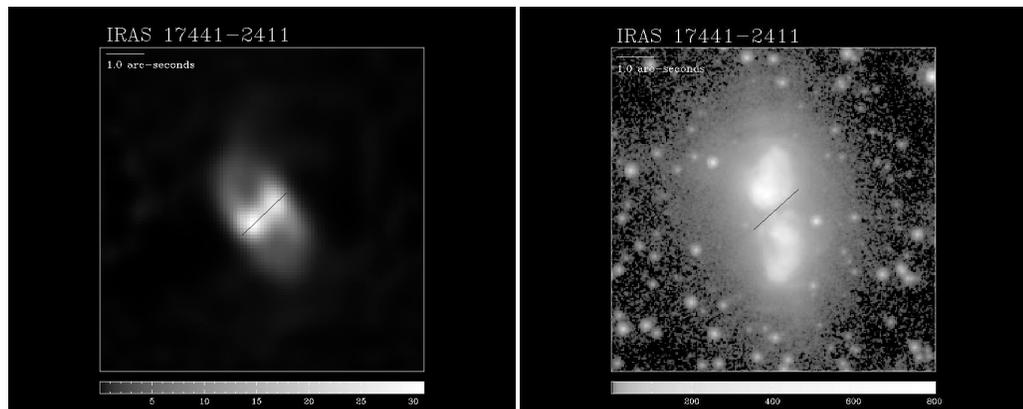
Fig. 3. Gemini T-ReCs 11.7 μm images of PPN IRAS $17441-2411$ (left). The orientation of the infrared disk is overlaid on the optical I band *HST* image (right) as a solid line [21].

4 Molecular Hydrogen and Shock Excitation

The 2.12 μm vibrational-rotational line of H_2 is a useful tracer of shock in PNe. Since this line lies in the K-band window, H_2 image of PNe can be obtained by near-infrared imaging with ground-based telescopes. Strong H_2 emission can be seen in the equatorial torus regions as well as in the bipolar lobes of IC 4406 and NGC 2346 (Fig. 4). A bright elliptical ring can clearly be seen in the waist of IC 4406. The bright rims in the lobes sharply define the edges of the lobes, suggesting that the lobes are confined by an external medium and that the H_2 emission trace regions of wind interaction. The H_2 emissions at the caps of the lobes probably represent the regions where the fast wind is breaking through the remnant AGB circumstellar envelope. Most interestingly, radial jets can be seen along the equatorial plane of IC 4406. Similar structures of equatorial torus, bipolar lobes, and radial equatorial jets can also be seen in K3-72 (Fig. 5). NGC 2440 shows an extended spherical molecular halo of $73''$ in diameter (Fig. 5). A bright rim of the halo probably traces the shock interaction between the halo and the ISM. It is interesting to note that the nebula is not located at the center of the spherical halo.
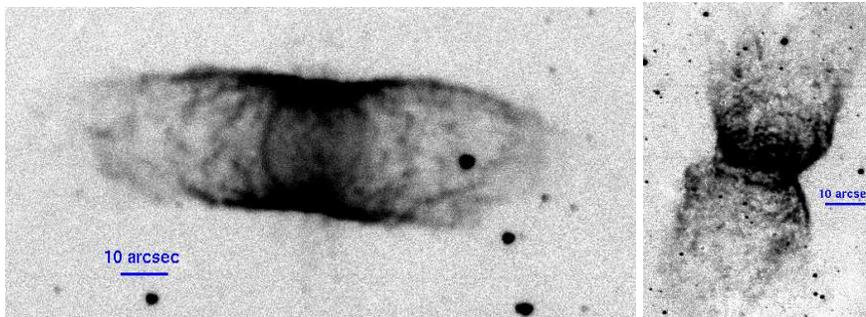
Fig. 4. Continuum-subtracted H_2 image of IC 4406 (left) and NGC 2346 (right).

5 The Intrinsic 3-D Structure of Planetary Nebulae

Beginning with the work of Curtis[1], there have been many attempts in classifying the morphologies of PNe. However, all classification schemes suffer from the following problems: (i) sensitivity dependence: where a deeper exposure reveals fainter structures which change the classification of the PNe; (ii) species dependence: where the morphology of PNe observed in lines of different ions differs as the result of ionization structures and stratification effects. and (iii) projection effects: morphology classifications describe the two-dimensional apparent structures, not the intrinsic 3-D structures of the PNe.
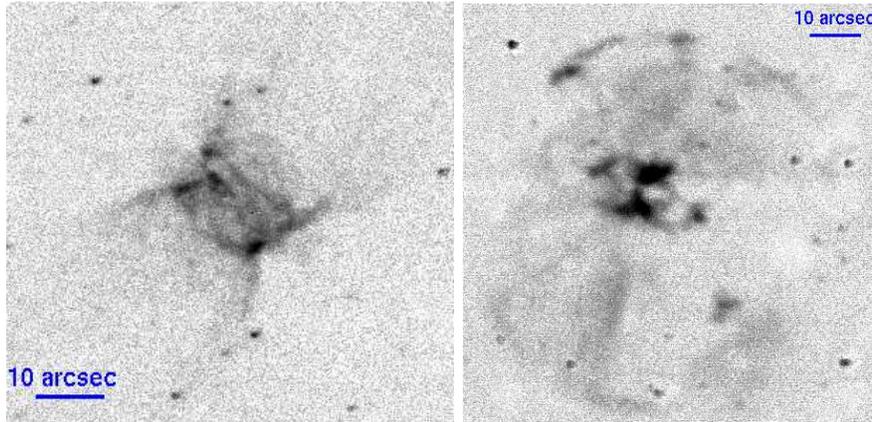
Fig. 5. Continuum-subtracted H_2 images of K3-72 (left) and NGC 2440 (right).

It is clear that the examination of the apparent morphology alone is not sufficient to obtain the true intrinsic structure of PN. Kinematic data are necessary to separate various components projected on the same positions in the sky. Comparisons between the 3-D kinematic model with imaging spectroscopy observations of PNe threrefore represent the best way to determine the true instrinsic 3-D structurre. An example of the modeling the Ring Nebula is given by Steffen et al. in these proceedings [18].

6 Origin of Diversity of PN Morphologies

The morphological features of PNe can be broadly classified into the following three catagories based on their degree of symmetry:

- Multiple shells: these represent uneven brightness distribution in the radial directions and include shells, rims, crowns, and haloes. Usually they represent spherical strucutres although in some cases the apparent multiple shells can be due to the projection of bipolar lobes and the torus onto the plane of the sky [18]. A series of roughly equally spaced circular arcs are observed in PNe and PPNe [9]. They are believed to be spherical shells beonging to the remnant of the AGB wind.
- Axial symmetric features: bipolar lobes and equatorial torus are the most common features of a bipolar (butterfly) nebula. Also belonging to this catagory are ansaes and FLIERS commonly seen in elliptical nebulae. Two-dimensional rings perpendicular to the bipolar axis have been seen in several PNe [6, 7].
- Point symmetric structures: these include S-shape structures, multiple lobes, and other morphological features better described by symmetry

relative to a central point rather than to an axis. In some cases, point symmtry can be attributed to precessing motions [11].

The general spherical symmetric structures such as shells, rims, crowns, and haloes can be understood by the dynamical processes of interacting winds coupled with time-dependent photoionization [16]. The origin of the concentric rings is not certain but could be related to the time-dependent nature of the AGB wind. FLIERS and 2-D rings could be the result of interaction between a time-variable fast outflow with the AGB wind [17, 7]. The problem on the origin of the point-symmetric structures is much more challenging. Hypotheses involving binary central stars and/or magnetic fields have been suggested as agents for precession.

7 Jets and Tori

Some PNe have extreme bipolar (cylindrical) shapes, suggesting that their morphology is shaped by a collimated outflow [15] (Fig. 6). In order to test the various collimation and outflow mechanisms, it would be desirable to be able to directly image the fast outflow ("jets") and the equatorial tori ("disks"). The tori can be imaged in scattered light (Fig. 6), in molecular and dust emission (sections 2 and 3) and the fast collimated outflow can be detected in optical emission lines, molecular emission and in free-free continuum emission [10]. If the mass loss rate and velocity of the fast collimated outflow can be determined, their values would have implications on the driving mechanism. For example, if the fast outflow is driven by accretion, then the observed mechanical luminosity must be smaller than the expected accretion rate.
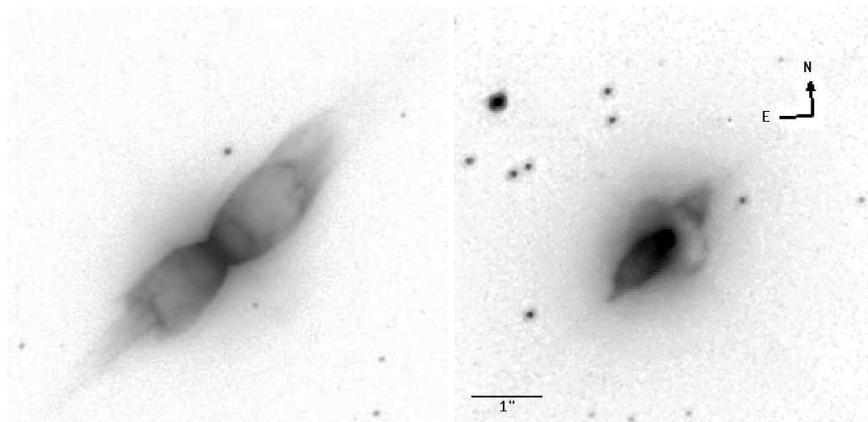
Fig. 6. Left: He2-320 is an example of PNe with highly collimated lobes. Right: A disk can clearby be seen in scattered light in the PPN IRAS 17106−3046 [8].

8 Summary

Recent infrared and submm observations of the dust and molecular gas components of PNe have identified the neutral torus region, which previously has only been seen as dark lanes in optical images. Dust and molecular emissions are also detected in the bipolar lobes, which can be used as direct tracer of the high-velocity collimated outflow.

9 Acknowledgements

References

1. H.D. Curtis: Publ. Lick Obs., Vol. XIII, Part III, p. 57 (1918)
2. Dinh-V-Trung, V. Bujarrabal, A. Castro-Carrizo, J. Lim, S. Kwok: ApJ, submitted
3. C. F. Gammie, G. R. Knapp, K. Young, T. G. Phillips, E. Falgarone: ApJ, **345**, L87 (1989)
4. J. F. Graham, E. Serabyn, T. M. Herbst, K., Matthews, G. Neugebauer, B. T. Soifer, T. D. Wilson, S. Beckwith: AJ, **105**, 250 (1993)
5. S. Kwok, K. Volk: ApJ **299**, 191 (1985)
6. S. Kwok, K.Y.L. Su: ApJ, **635**, L49 (2005)
7. S. Kwok, C.H. Hsia: ApJ, **660**, 341 (2007)
8. S. Kwok, B.J. Hrivnak, K.Y.L. Su: ApJ Letters, **544**, L149 (2000)
9. S. Kwok, K.Y.L. Su, J.A. Stoesz: in *Post-AGB Objects as a Phase of Stellar Evolution*, ed by R. Szczerba, S.K. Górny, (Kluwer 2001), pp 115
10. T.H. Lee, J. Lim, S. Kwok: ApJ, **665**, 341 (2007)
11. L.F. Miranda, M. Guerrero, J.M. Torrelles: AJ, **117**, 1421 (1999)
12. C. Muthumariappan, S. Kwok, K. Volk: ApJ **640**, 353 (2006)
13. J. Nakashima, et al.: AJ, in press
14. N. Peretto, G.A. Fuller, A.A. Zijlstra, N.A. Patel: A&A, in press
15. R. Sahai, V. Bujarrabal, A. Zijlstra: ApJ **518**, L115 (1999)
16. D. Schönberner, R. Jacob, M. Steffen, M. Perinotto, R.L.M. Corradi, A. Acker: A&A **431**, 963 (2005)
17. W. Steffen, J.A. López, A. Lim: ApJ **556**, 823 (2001)
18. W. Steffen, J. A. López, N. Koning, S. Kwok, H. Risgo, M.G. Richer, C. Morisset, these proceedings
19. K. Y. L. Su et al.: ApJ Suppl. **154**, 302 (2004)
20. M.Y. Wang, T. Hasegawa, S. Kwok: ApJ, submitted
21. K. Volk, S. Kwok: ApJ, in press
22. K., Volk, B.J. Hrivnak, K.Y.L., Su, K.Y.L., S. Kwok: ApJ **651**. 204 (2006)